PHYSICAL REVIEW B VOLUME 25, NUMBER 6 15 MARCH 1982

Wannier-Mott excitons in semi-infinite crystals: Wave functions and normal-incidence reflectivity

A. D'Andrea
Laboratorio di Metodologie Avanzate Inorganiche, Consiglio Nazionale delle Ricerche, Rome, Italy

R. Del Sole
Gruppo Nazionale di Struttura della Materia-Consiglio Nazionale delle Ricerche, Instituto di Fisica, Università di Roma, Rome, Italy

(Received 19 January 1981)

A method is developed to obtain Wannier-Mott—exciton wave functions in semi-infinite crystals in the framework of the effective-mass approximation. An analytical approximation is shown to agree well with numerical wave functions and is used to compute exciton nonlocal polarizability (in closed form) and *s*-wave reflectivity. The results are compared with normal-incidence reflectivity experiments in CdS, ZnSe, GaAs, and InP, and the experimental line shapes are well reproduced. The existence of an intrinsic dead layer is confirmed and a new additional boundary condition is derived. It is shown that the spike, frequently observed at the longitudinal-exciton frequency, is due to extrinsic dead layers.

I. INTRODUCTION

The effect of spatial dispersion on exciton optical properties is not yet completely understood. Since two polariton branches[1] propagate in the presence of spatial dispersion, an additional boundary condition (ABC) is needed to determine their relative amplitude, in addition to Maxwell's boundary conditions. In their pioneering work, Hopfield and Thomas[2] showed the exciton polarization to vanish at the surface, as already hypothesized by Pekar,[1] in the case of a tight-binding model of Frenkel excitons with nearest-neighbor interactions. They also introduced the concept of dead layer in order to account for the repulsive image potential that extended excitons feel near the surface. Since then, the correct ABC and the existence of the dead layer have been the object of a not-yet-settled controversy.

It is clear that the ABC and an eventual dead layer must be embodied in the nonlocal nonhomogeneous dielectric susceptibility of the vacuum-crystal system. This was shown first in the framework of the so-called dielectric approximation,[3–5] which assumes that the bulk, translationally invariant, dielectric susceptibility $\epsilon(\omega, \vec{r}-\vec{r}')$ holds up to the surface. This approximation leads to an ABC different from that of Pekar[1] and Hopfield and Thomas[2] and to no dead layer, but seems quite unphysical, since it completely neglects surface effects.

Further insight was provided by some papers[6,7] dealing with the relation between the kind of exciton reflection at the surface and ABC. In general, exciton reflection at the surface leads to a nonhomogeneous dielectric susceptibility. The dielectric approximation results to be a particular case, corresponding to diffuse reflection. These papers, however, neglect the effect of the surface on exciton internal motion, limiting themselves to the case of Frenkel excitons. In recent years these have been studied in great detail in a number of papers[8–11] where microscopic calculations of optical properties have been carried out for quite sophisticated models. Pekar's ABC has been confirmed in the case of semi-infinite isotropic crystals.[8]

On the other hand, microscopic calculations for extended (Wannier-Mott) excitons have also been performed.[12–15] The existence of a transition region near the surface, where excitons are less probably found than in the bulk (dead layer), is confirmed, but the use of the adiabatic approximation[13,14] which is questionable for values of the ratio M/μ of the exciton total mass to the reduced mass of order 10, as encountered in most semiconductors, or too many other approximations in some

calculations[12,15] make the results only qualitatively correct. A further shortcoming of the adiabatic approximation approach is that cumbersome calculations are needed in order to compute reflectance line shapes, and therefore these are computed only in specific cases (equal electron and hole masses,[13] for instance) and comparison with experiments is made[14] approximating the above-mentioned transition region with a homogeneous dead layer without excitons.

A number of experiments have been performed[16–24] and interpreted in terms of a homogeneous dead layer and various ABC's. It has been shown[17] that any ABC gives a good fit of normal-incidence reflectivity if the dead layer depth is a fitting parameter, while oblique incidence reflectivity seems to favor Pekar's ABC.[22] A further complication arises, since extrinsic dead layers often exist in semiconductors, due, for instance, to built-in electric fields which may ionize excitons. Extrinsic dead layers, much larger than the exciton radius, have also been hypothesized in solid rare gases.[25] For these reasons, dead layer depths determined by fitting experimental line shapes are not conclusive, and further theoretical work is required in order to have a full understanding of the behavior of extended excitons near the crystal boundary.

The purpose of this paper is to formulate the problem more rigorously. In Sec. II we compute Wannier-exciton wave functions in a semi-infinite crystal avoiding the use of the adiabatic approximation. The image potential is neglected in order to make the calculation feasible. This approximation is justified in Sec. II. We believe that it does not substantially lower the accuracy of our results which should remain at least semiquantitatively correct. A simple approximate wave function, whose correctness is tested by comparison with numerical calculations, is employed to compute exciton polarizability in closed form in Sec. III. In Sec. IV we solve the equation of light propagation for an s wave. In Sec. V we compute normal-incidence reflectivity that can be made to agree with experimental line shapes in a number of semiconductors by varying only a few parameters. The approximations involved in calculations and the results obtained are discussed in Sec. VI. We find that the exciton polarization vanishes at the surface, in agreement with Pekar[1] and Hopfield and Thomas,[2] and that there is a transition region, roughly speaking, the dead layer, where excitons are less probably found than in bulk. We find also a new ABC, depending on exciton size and oscillator strength, that determines the relative amplitudes of the two polariton branches. A partial account of this work has already been published elsewhere.[26]

II. EXCITON WAVE FUNCTIONS

A. Effective-mass Hamiltonian and boundary conditions

We consider excitons at the fundamental edge of a semiconductor with parabolic nondegenerate valence and conduction bands, occupying the half-space $z>0$. The effective-mass Schrödinger equation is

$$\left[-\frac{\hbar^2}{2M}\Delta_R-\frac{\hbar^2}{2\mu}\Delta_r-\frac{e^2}{\epsilon r}+V_{\rm im}(\vec{r},Z)\right]\Phi(\vec{r},\vec{R}) =E\Phi(\vec{r},\vec{R}) , \quad (1)$$

where $\vec{R}$ is the center-of-mass position, $\vec{r}=\vec{r}_e-\vec{r}_h$, $\vec{r}_e=(\vec{\rho}_e,z_e)$, and $\vec{r}_h=(\vec{\rho}_h,z_h)$ are the electron and hole position, respectively, and the exciton energy E is measured from the conduction-band bottom. The image potential is[13]

$$V_{\rm im}(\vec{r},Z)=-\frac{e^2}{\epsilon}\frac{\epsilon-1}{\epsilon+1} \times\{[(\vec{\rho}_e-\vec{\rho}_h)^2+(z_e+z_h)^2]^{-1/2} -(4z_e)^{-1}-(4z_h)^{-1}\} , \quad (2)$$

ϵ being the bulk dielectric constant. We assume throughout this paper the boundary condition (BC) that the envelope wave function $\Phi(\vec{r},\vec{R})$ vanishes when either the electron or the hole are at the surface:

$$\Phi(z_e=0)=\Phi(z_h=0)=0 . \quad (3)$$

This boundary condition has been shown to be correct in absence of surface states when a large surface barrier prevents electron and hole escape from the surface[27,28] and has been used for explaining surface effects on electroreflectance.[29,30] It has also been derived[31] from the image potential infinite barrier that electrons and holes experience approaching the surface [see Eq. (2)] and has been assumed in previous works[12–15] on the argument of the present paper. The boundary conditions (3) are, however, questionable in presence of surface states. Recently a tight-binding model of excitons

near solid surfaces has been developed by Altarelli *et al.*[32] neglecting the hole motion and the image potential. A layer with exciton binding energy smaller than in bulk (dead layer) is found in absence of surface states, in agreement with calculations founded on Eq. (3) and the adiabatic approximation.[13,14] However, when empty (filled) surface states are present below (above) or near the conduction-band bottom (valence-band top), an increase of exciton binding energy near the surface is found, in contrast with the results derived from Eq. (3). However, this BC could be valid also in the presence of surface states for the effect of the image potential neglected in Ref. 32, which could prevent carriers from approaching the surface. Though the validity of (3) is an open question, we assume it in this paper, neglecting in this way the microscopic structure of the surface.

In order to make the problem of finding wave functions tractable when the adiabatic approximation is not used, we are forced to neglect the image potential in (1). We show below that this does not lead to serious errors if BC (3) is used. Actually this BC has roughly the same effect as the image potential on electron and hole motion, since it repels both from the surface. Calculations[14] in the framework of the adiabatic approximation have shown that the inclusion of the full image potential in addition to BC (3) has little effect. A further argument not founded on the adiabatic principle is that the image potential is small when the electron-hole separation is smaller than the distance from the surface. The solid lines in Figs. 1 and 2 show the ratio of the image potential to the Coulomb energy, computed when the electron-hole distance is equal to the exciton radius a_B, as a function of the center of mass distance from the surface Z, for CdS and InP, respectively. This ratio is smaller than 0.1 for Z larger than the exciton radius a_B. Since the BC (3) repels excitons to a distance from the surface much larger than a_B, as will be shown later, the image potential can be neglected. Therefore, in this section, we are going to solve Eq. (1) with boundary condition (3) and

$$V_{\rm im}(\vec{r},Z)=0\ . \tag{2'}$$

B. Formal solution

Equation (1) is separable in $\vec{r}$ and $\vec{R}$, but a single-product wave function does not satisfy the boundary conditions (3). Then we write the solution as a linear combination of product wave functions, each being a solution of (1) with the same total energy E, that however is differently shared between internal and center-of-mass motion:

$$\Phi(\vec{r},\vec{R})=\frac{1}{2\pi}\exp(i\vec{K}_{||}\cdot\vec{R}_{||})\psi(\vec{r},Z)\ , \tag{4}$$

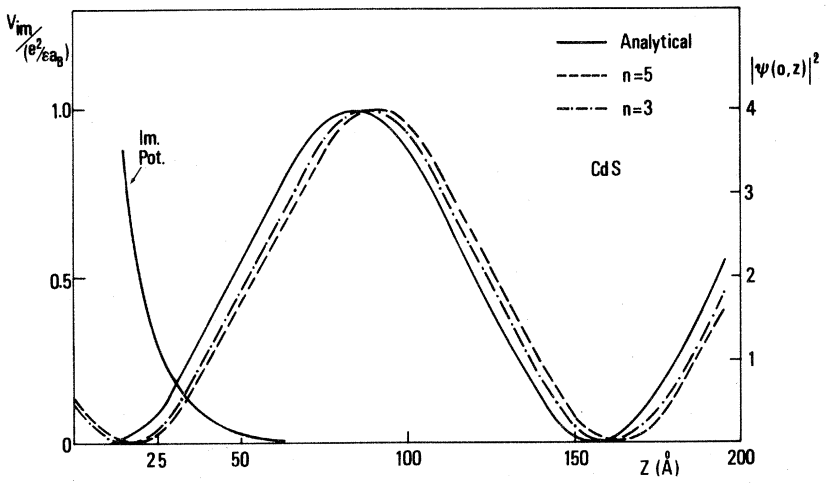

FIG. 1. CdS. Right-hand scale: exciton oscillator strength $|\psi(0,Z)|^2$ in units of $|\varphi_1(0)|^2/2\pi$ as function of the center-of-mass depth Z, for E_B (center-of-mass energy)=2 meV. The analytical approximation, computed according to Eq. (20) is compared with variational wave functions, computed as shown in Sec. II C, including exciton states up to $n=3$ and $n=5$. Left-hand scale: the ratio of the image potential to the Coulomb potential computed for electron-hole separation equal to a_B, and $z_e-z_h=a_B/\sqrt{3}$. We choose the case where the hole is nearer to the surface ($z_e>z_n$) since it yields a larger image potential.

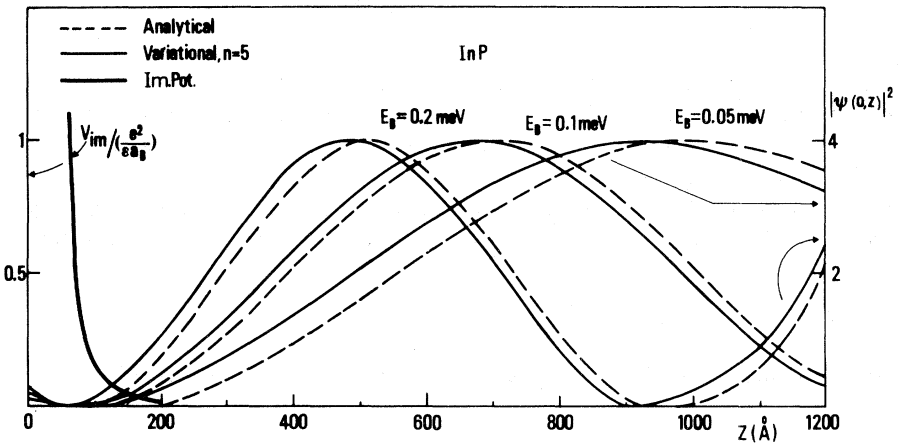

FIG. 2. InP. Right-hand scale: exciton oscillator strength $|\psi(0,Z)|^2$ in units of $|\varphi_1(0)|^2/2\pi$, computed as function of the center-of-mass depth Z, for $E_B=0.05$, 0.1, and 0.2 meV. The analytical approximation, computed according to Eq. (20), is compared with variational wave functions, computed as shown in Sec. II C, including exciton states up to $n=5$. $E_r<0.02$ for all variational wave functions. Left-hand scale: image potential, computed and normalized as in Fig. 1.

$$\psi(\vec{r},Z)=[\pi(1+|A|^2)]^{-1/2} \times\left[[\exp(-iK_zZ)+A\exp(iK_zZ)] \times\varphi_1(r)+\sum_n c_n\varphi_n(\vec{r})\exp(-P_nZ)\right], \tag{5}$$

where $\varphi_1(r)$ and $\varphi_n(\vec{r})$ are respectively, the ground state and excited hydrogenic wave functions with energy E_n, $\mathscr{E}=E-\hbar^2K_{||}^2/2M_{||}$, $\vec{K}=(\vec{K}_{||},K_z)$, $K_z>0$, is the center-of-mass wave vector, such that $\mathscr{E}=-R^*+\hbar^2K_z^2/2M_\perp$, R^* is the effective Rydberg, and

$$P_n=[2M_\perp(E_n-\mathscr{E})/\hbar^2]^{1/2}. \tag{6}$$

$M_{||}$ and $M_\perp$ are, respectively, the exciton mass parallel and perpendicular to the surface plane. We are considering solutions with E greater than $E_1=-R^*$, and smaller than $E_2=-R^*/4$, so that oscillating center-of-mass wave functions occur only together with φ_1. The internal motion wave functions are those of the hydrogen atom, since they must be regular as r tends to zero and to infinity. The cylindrical symmetry around the z axis allows the azimuthal quantum number m to be the same for all terms in the sum in (5). We restrict ourselves to the case $m=0$, since only such excitons are optically allowed.[33] The wave function (4) is correctly normalized, as shown in the Appendix.

The c_n's and A must be found imposing the boundary conditions (3), namely that wave function vanishes at $z=M_\perp Z/m_e$ ($z_e=0$), and at $z=-M_\perp Z/m_h$ ($z_h=0$). Substituting for Z in Eq. (5), we find that the function

$$F(\vec{r})=\left[\varphi_1(r)\{\exp[-iK_zs(z)|z|]+A\exp[iK_zs(z)|z|]\}+\sum_n c_n\varphi_n(\vec{r})\exp[-P_ns(z)|z|]\right]\Big/[\pi(1+AA^*)]^{1/2}, \tag{7}$$

where $s(z)=m_e/M_\perp$ for $z>0$, and $s(z)=m_h/M_\perp$ for $z<0$, must be identically zero, in order to satisfy Eq. (3). If we multiply by the hydrogenic wave functions $\varphi_k(r)$, which are a complete set in the r space and integrate over all space, we find the system

$$A\langle k|\exp[iK_zs(z)|z|]|1\rangle+\sum_n c_n\langle k|\exp[-P_ns(z)|z|]|n\rangle=-\langle k|\exp[-iK_zs(z)|z|]|1\rangle.$$

There is an equation and an unknown c_n (A for the ground state) for each hydrogen state n, so that the nonhomogeneous system has at least one solution. In the following section we will show practical methods to find the wave functions.

C. Variational approach

In order to carry out practical calculations, it is unavoidable to retain only a finite number of hydrogenic excited states in the sum in Eq. (5). In this case, the wave function is still an exact solution of the Schrödinger equation, but the boundary conditions (3) cannot be rigorously satisfied. A similar problem is present in the cellular method of band calculation.[34]

We look for wave functions that minimize the mismatch of the boundary condition, namely the function $F(\vec{r})$, Eq. (7), that should be zero if the BC (3) were rigorously satisfied. Therefore, we try to fulfill the condition

$$\int_{\vec{r}\ \text{space}} d^3r \mid F(\vec{r}) \mid^2 = \min . \tag{3'}$$

We require that the derivatives of (3') with respect to c_n^* and A^* vanish. We get

$$\sum_m c_m M_{nm} = -T_n(-K_z) - AT_n(K_z) , \tag{8}$$

$$A^2 \left[f(K_z) + \sum_m c_m^* T_m(K_z) \right] + A \left[\sum_{nm} M_{nm} c_n^* c_m + \sum_m c_m T_m^*(-K_z) + \sum_m c_m^* T_m(-K_z) \right] = f(-K_z) + \sum_m c_m T_m^*(K_z) , \tag{9}$$

with

$$M_{nm} = \langle n \mid \exp[-s(z) \mid z \mid (P_n + P_m)] \mid m \rangle , \tag{10}$$

$$T_n(K_z) = \langle n \mid \exp[s(z) \mid z \mid (iK_z - P_n)] \mid 0 \rangle , \tag{11}$$

and

$$f(K_z) = \langle 0 \mid \exp[2is(z) \mid z \mid K_z] \mid 0 \rangle . \tag{12}$$

Here n and m label *excited* hydrogenic states, and $\mid 0 \rangle$ the ground state. We multiply Eqs. (8) by c_n^* and sum them over n, then substitute into the second set of large parentheses of the left-hand side of Eq. (9) and get

$$A^2 f(K_z) + A \sum_m c_m T_m^*(-K_z) = f(-K_z) + \sum_m c_m T_m^*(K_z) . \tag{13}$$

Now we solve the system (8), inverting the matrix M_{nm}:

$$c_n = -\sum_m (M^{-1})_{nm} [T_m(-K_z) + AT_m(K_z)] .$$

Insertion of the solution into (13) yields

$$A^2 [f(K_z) - h(K_z)] = f^*(K_z) - h^*(K_z) , \tag{14}$$

where

$$h(K_z) = \sum_{nm} (M^{-1})_{nm} T_n(K_z) T_m(K_z) . \tag{15}$$

In deriving (14), we have taken advantage of the reality of the hydrogenic wave functions involved, namely those with $m=0$. The solution of (14) which minimizes (3') is

$$A = -\mid f(K_z) - h(K_z) \mid / [f(K_z) - h(K_z)] , \tag{16}$$

giving

$$\int d^3r \mid F(\vec{r}) \mid^2 = \pi^{-1} \left[1 - \mid f(K_z) - h(K_z) \mid - \sum_{nm} (M^{-1})_{nm} T_n(K_z) T_m^*(K_z) \right] . \tag{17}$$

In order to check the validity of the approach, we compare the integrated mismatch of boundary condition (17) with that of the bulk exciton wave function. This is $1/\sqrt{\pi}\varphi_1(r)\exp(i\vec{K}\cdot\vec{R})$, normalized to $\delta(\vec{K}-\vec{K}')$ in the half-space $z>0$, and yields a boundary mismatch $1/\pi$. Therefore, the validity of the present method requires the error, Eq. (17), to be much smaller than $1/\pi$, namely

$$E_r = 1 - \mid f(K_z) - h(K_z) \mid - \sum_{nm} (M^{-1})_{nm} T_n(K_z) T_m^*(K_z) << 1 .$$

We consider the case of CdS in order to show the convergence of the method. Figure 1 reports $\mid \psi(0,Z) \mid^2$, that is proportional to the exciton oscillator strength (see Sec. III), in the case E_B

$=\hbar^2K_z^2/2M_\perp=2$ meV for various truncations of the sum in Eq. (5). If only the $n=2$ level is included, $E_r=0.088$, already valuably smaller than 1. Inclusion of the levels up to $n=4$ reduces E_r to 0.034, while the level $n=5$ leads to a little improvement ($E_r=0.032$). We conclude that the inclusion of a few hydrogenic states, from 10 ($n=4$) to 15 ($n=5$) gives quite accurate wave functions with boundary mismatch E_r of the order of 0.03. Calculations for smaller values of E_B and different materials (GaAs, InP, ZnSe) give similar or even better results.

D. Analytical approximation

The method of the preceding section involves extensive numerical calculations and is not practical for computing optical properties. We show here a simple analytical approximation that we will check by comparison with the numerical calculations. This approximation has already been reported in detail in Ref. 26, but we prefer to repeat it for the sake of completeness and in order to correct some print errors of Ref. 26.

The analytical approximation can be derived under the assumption that the c_n's rapidly approach zero above the exciton ionization edge. In this case, the relevant E_n's in Eq. (5) range from $E_2=-R^*/4$ to about zero, so that $E_n-\mathscr{E}$ and P_n are nearly constant, the latter ranging from $(3R^*M_\perp/2\hbar^2)^{1/2}$ to $(2R^*M_\perp/\hbar^2)^{1/2}$, if $\mathscr{E}$ is very close to $-R^*$. This allows one to replace the P_n's in Eq. (5) by some mean value P, for not too large Z and $M_\perp$ values.[35]

The use of boundary conditions (3) yields:

$$f(\vec{r})\equiv\sum_n c_n\varphi_n(\vec{r})=\begin{cases}-\varphi_1(r)[\exp(-iK_zm_ez/M_\perp)+A\exp(iK_zm_ez/M_\perp)]\exp(m_ePz/M_\perp) & \text{for } z>0\\ -\varphi_1(r)[\exp(iK_zm_hz/M_\perp)+A\exp(-iK_zm_hz/M_\perp)]\exp(-m_hPz/M_\perp) & \text{for } z<0\,.\end{cases} \tag{18}$$

$f(\vec{r})$ is continuous at $z=0$, and also $\partial f(\vec{r})/\partial z$ must be continuous, leading to

$$A=-(P-iK_z)(P+iK_z)^{-1}\,. \tag{19}$$

The final result for $\psi(0,Z)$, that is relevant for calculation of the dielectric susceptibility, is

$$\psi(0,Z)=(2\pi)^{-1/2}\varphi_1(0)\times[\exp(-iK_zA)+A\exp(iK_zZ)-(1+A)\exp(-PZ)]\,. \tag{20}$$

Equations (5) and (20) describe an exciton traveling with momentum $-\hbar K_z$ towards the surface, being completely ($|A|^2=1$) back reflected, together to an evanescent wave localized in a depth $\sim 1/P$ near the surface. The choice of P in the previously mentioned range has practically no effect on wave functions and we choose $P=(2M_\perp R^*/\hbar^2)^{1/2}$.

Hence, the transition region depth is about

$$l=P^{-1}\simeq(\mu/M_\perp)^{1/2}a_B\,, \tag{21}$$

of the order of one half of the exciton Bohr radius for the relevant values of $\mu/M_\perp$. After the transition region,

$$\psi(0,Z)=-2(2\pi)^{-1/2}i\sin[K_z(Z-l)]\varphi_1(0)\,, \tag{20'}$$

provided A is expanded up to first order in K_z/P. This is the same behavior of excitons starting after a dead layer of depth l with boundary condition $\psi(0,l)=0$. For this reason, we will often call l the dead layer depth, but it must be emphasized that we are dealing with a continuous transition region and by no means with a homogeneous dead layer.

We were not able to show the validity of the main assumption of this subsection, namely that the c_n's are rapidly approaching zero above the exciton ionization edge. Thus, we check the analytical approximation by comparison with the numerical wave functions computed as shown in the preceding section. The solid line in Fig. 1 is the analytical approximation to $|\psi(0,Z)|^2$ in CdS for $E_B=2$ meV, that well agrees with numerical curves. Figure 2 reports comparison between analytical and numerical wave functions in the case of InP for various values of E_B. It is clear also from calculations appropriate to different cases that the analytical approximation gives quite accurate wave functions, embodying the essential physics of the problem. The initial ranges in Figs. 1 and 2 where $|\psi(0,Z)|^2$ is very small, of about 10 Å in CdS and 100 Å in InP, yield a striking evidence of the dead layer.

The image potential, computed for electron-hole separation equal to a_B, has been plotted in Figs. 1 and 2 (solid lines). It is small with respect to the Coulomb interaction when the exciton wave func-

tion is appreciably different from zero, so that it is justified to neglect it.

In conclusion, we have shown that the analytical wave function (20) is a suitable approximation to the exact exciton wave function in presence of the boundary conditions (3). We will use it in the following sections in order to compute exciton reflectivity.

III. EXCITON POLARIZABILITY

The polarization $\vec{P}(\vec{R})$ at a site $\vec{R}$ is related to the macroscopic electric field $\vec{E}(\vec{R})$ through the nonlocal polarizability $\chi(\vec{R},\vec{R}')$:

$$\vec{P}(\vec{R})=\int d^3R'\chi(\vec{R},\vec{R}')\vec{E}(\vec{R}') .$$

Both $\vec{P}(\vec{R})$ and $\vec{E}(\vec{R})$ are cell-averaged quantities, and $\chi(\vec{R},\vec{R}')$ is assumed to be a scalar quantity. In the framework of linear response theory, $\chi(\vec{R},\vec{R}')$ is given by[6]

$$\chi(\vec{R},\vec{R}',\omega)=\chi_0(\omega)\delta(\vec{R}-\vec{R}')\Theta(Z)\Theta(Z')+\omega^{-2}\sum_{\nu}\left[\frac{\langle 0|j(\vec{R})|\nu\rangle\langle\nu|j(\vec{R}')|0\rangle}{E_\nu+(\hbar\omega+i\Gamma)}+\frac{\langle 0|j(\vec{R}')|\nu\rangle\langle\nu|j(\vec{R})|0\rangle}{E_\nu-(\hbar\omega+i\Gamma)}\right] \tag{22}$$

where $|0\rangle$ is the crystal ground state, ν labels the relevant excited states, namely the exciton branch of interest, with excitation energy E_ν, and $\chi_0(\omega)$ is the nonresonant polarizability, including the contribution of higher-energy transitions, that is assumed not to be affected by spatial dispersion. Γ is the exciton lifetime broadening, and $j(\vec{R})$ is the cell-averaged density-current operator (in the direction of the electric field), whose matrix elements can be computed from exciton wave functions, as described in the following.

The exciton state $|\nu\rangle$ can be expanded in Wannier functions according to

$$|\nu\rangle=\Omega\sum_{\vec{R}_e\vec{R}_h}\Phi_\nu(\vec{R}_e,\vec{R}_h)|\vec{R}_e\vec{R}_h\rangle , \tag{23}$$

where Ω is the cell volume, $\Phi(\vec{R}_e,\vec{R}_h)$ the exciton wave function normalized as in Sec. II and $|\vec{R}_e,\vec{R}_h\rangle$ is the state where an electron occupies the conduction-band Wannier state at $\vec{R}_e$ and a hole is in the valence-band Wannier function at $\vec{R}_h$. The cell-averaged density-current operator matrix element is

$$\langle 0|j(\vec{R})|\nu\rangle=-i\hbar e(2m)^{-1}\sum_{(\vec{R}_e\vec{R}_h)}\Phi_\nu(\vec{R}_e,\vec{R}_h)\int_{\text{cell }\vec{R}}d^3r[a_v^*(\vec{r}-\vec{R}_h)\hat{e}\cdot\vec{\nabla}a_c(\vec{r}-\vec{R}_e) - a_c(\vec{r}-\vec{R}_e)\hat{e}\cdot\vec{\nabla}a_v^*(\vec{r}-\vec{R}_h)] , \tag{24}$$

where $\hat{e}$ is the versor of the electric field and $a_v(\vec{r})$ and $a_c(\vec{r})$ are, respectively, valence- and conduction-band Wannier functions.

The integral is clearly different from zero only if $\vec{R}_e$ and $\vec{R}_h$ are very close to $\vec{R}$, because of the local character of Wannier functions, so that we may replace the smooth effective-mass function $\Phi(\vec{R}_e,\vec{R}_h)$ with its value at $\vec{R}_e=\vec{R}_h=\vec{R}$ and get

$$\langle 0|j(\vec{R})|\nu\rangle=-ie\hbar(2m)^{-1}\Phi_\nu(\vec{R},\vec{R})\sum_{\vec{R}_c\vec{R}_h}\int_{\text{cell }\vec{R}}d^3r[a_v^*(\vec{r}-\vec{R}_h)\hat{e}\cdot\vec{\nabla}a_c(\vec{r}-\vec{R}_e) - a_c(\vec{r}-\vec{R}_e)\hat{e}\cdot\vec{\nabla}a_v^*(\vec{r}-\vec{R}_h)] . \tag{25}$$

Using the $k=0$ Bloch functions $u_c(\vec{r})$ and $u_v(\vec{r})$, this can be written as

$$\langle 0|j(\vec{R})|\nu\rangle=(e/m)\Phi_\nu(\vec{r}=0,\vec{R})P_{vc} , \tag{26}$$

where Φ_ν is expressed as function of the electron-hole relative coordinate $\vec{r}$ and center-of-mass coordinate $\vec{R}$, and

$$p_{vc}=\int_{\text{cryst}} d^3r\, u_v^*(r)\hat{e}\cdot\vec{P}u_c(r) \tag{27}$$

is the momentum-operator matrix element.

The density-current operator matrix element is proportional to the probability amplitude of finding electron and hole at the same site, as it is well known in the case of infinite crystals.[33] We have restated the result in the case of crystals with surface where translational invariance perpendicular to the surface is missing, because we did not find a satisfactory derivation in the literature.

Inserting Eq. (26) into (22), using (4), and multiplying by 2 in order to account for spin degeneracy, we find for the exciton polarizability, Fourier transformed in the xy plane:

$$\chi(K_{||},Z,Z')=\chi_0(\omega)\delta(Z-Z')+2e^2|p_{vc}|^2/(m^2\omega^2)$$

$$\times\sum_n\int_0^\infty dK_z\left[\frac{\psi_{nK_z}(0,Z)\psi^*_{nK_z}(0,Z')}{E_n+\hbar^2K_{||}^2/2M_{||}+\hbar^2K_z^2/2M_\perp-\hbar\omega-i\Gamma}+\frac{\psi_{nK_z}(0,Z')\psi^*_{nk_z}(0,Z)}{E_n+\hbar^2K_{||}^2/2M_{||}+\hbar^2K_z^2/2M_\perp+\hbar\omega+i\Gamma}\right] \tag{28}$$

for Z and $Z'>0$. Here n labels the states of exciton internal motion and $\vec{K}_{||}$ is the surface-plane projection of the light wave vector. Since we are interested in ω values near the $n=1$ exciton frequency $\omega_0=(E_g-R^*)/\hbar$, we consider explicitly in the integral only the first (resonant) term in large parentheses for $n=1$ and include other contributions into the background term χ_0. Furthermore, we use for $\psi_{nK_z}(0,Z)$ the analytic expression (20), that is valid only for small k_z values. This is justified since the difference between (20) and the correct wave function, being appreciable only at large K_z, when both denominators of (28) are nonresonant, gives a nonresonant contribution to polarizability, which is included in χ_0. After this, one recognizes, using Eqs. (19) and (20), that the integrand in (28) is an even function of K_z, and the integral can be extended to $-\infty$. The integral can then be easily computed by extension to the complex-K_z plane and by the method of residui. After simple algebra, the result is

$$\begin{aligned}\chi(K_{||},Z,Z')=&\chi_0(\omega)\delta(Z-Z')+i\alpha_0M_\perp\omega_0/(2\hbar q)\\&\times(\exp(iq|Z-Z'|)+(q+iP)(q-iP)^{-1}\exp[iq(Z+Z')]-2q(q-iP)^{-1}\\&\times\{\exp(iqZ-PZ')+\exp(iqZ'-PZ)-\exp[-P(Z+Z')]\}),\end{aligned} \tag{29}$$

with

$$q=[2M_\perp(\hbar\omega-\hbar\omega_0-\hbar^2K_{||}^2/2M_{||}+i\Gamma)/\hbar^2]^{1/2},\quad(\mathrm{Im}q>0), \tag{30}$$

and

$$\alpha_0=2e^2|P_{vc}|^2|\varphi_1(0)|^2/(m^2\omega^2\hbar\omega_0). \tag{31}$$

It is clear from (29) that the resonant exciton polarizability vanishes if either Z or Z' are zero as a direct consequence of boundary condition (3). This clearly demonstrates the validity of Pekar's ABC in the case of Wannier excitons at the surface (not below the dead layer, as generally assumed[16,17]).

Although it is incorrect to use the effective-mass approximation in the case of Frenkel excitons, Eq. (3) yields the correct result also in this case. In fact, the Frenkel-exciton limit can be obtained when R^* (and P) tends to ∞. In this case (29) reduces to

$$\chi_F(K_{||},Z,Z')=\chi_0(\omega)\delta(Z-Z')+i\alpha_0\omega_0M_\perp(2\hbar q)^{-1}\{\exp(iq|Z-Z'|)-\exp[iq(Z+Z')]\}, \tag{32}$$

which is the same result derived by Zehyer *et al.*[6] and Johnson and Rimbey[7] for Frenkel excitons using Pekar's ABC.

As Z or Z' tend to ∞, only the first exponential within the bold parentheses of Eq. (29) is nonvanishing due to the positive imaginary part of q. Therefore, $\chi(Z,Z')$ becomes a function of $|Z-Z'|$, as it must in the bulk, and its Fourier transform is

$$\chi(K_{||},K_z)=\chi_0(\omega)+\frac{\frac{1}{2}\alpha_0\hbar\omega_0}{[\hbar\omega_0+\hbar^2K_{||}^2/2M_{||}+\hbar^2K_z^2/2M_\perp-(\hbar\omega+i\Gamma)]} . \tag{33}$$

If we extract from χ_0 a nonresonant term

$$\frac{\frac{1}{2}\alpha_0(\hbar\omega_0)}{\hbar\omega_0+\hbar^2K_{||}^2/2M_{||}+\hbar^2K_z^2/2M_\perp+\hbar\omega+i\Gamma} ,$$

analogous to the second term in large parentheses in Eq. (28), to be added to the second term of Eq. (33), and compute the dielectric constant $\epsilon=1+4\pi\chi$ we find

$$\epsilon(\omega,K_{||},K_z)=\epsilon_0+\frac{4\pi\alpha_0(\hbar\omega_0)^2}{[(\hbar\omega_0+\hbar^2K_{||}^2/2M_{||}+\hbar^2K_z^2/2M_\perp)^2-(\hbar\omega+i\Gamma)^2]} , \tag{34}$$

with $\epsilon_0=1+4\pi\chi_0$, that agrees with Eq. (25) of Ref. 3, if $M_{||}=M_\perp$ is assumed and terms of the order K^4 are neglected. This shows that α_0 defined in Eq. (32) from microscopic quantities is the same as the exciton polarizability α of Ref. 2 and allows comparison of fitted α_0 values with those quoted in the literature.

IV. LIGHT PROPAGATION: *s* WAVE

In this paper we shall consider the case of normal incidence reflectivity. However, in this section we solve Maxwell's equations in the more general case of obliquely incident *s* wave, since it can be done with no further effort.

We consider *s* light polarized in the *y* direction propagating inside the crystal ($Z>0$). The electric field is of the form:

$$\mathscr{E}_y(X,Z)=E_y(Z)\exp(iK_{||}X) , \tag{35}$$

where $K_{||}=\omega\sin\theta/c$, and θ is the angle of incidence. Inserting (35) and (29) into the light-propagation equation, we obtain

$$\frac{d^2E_y(Z)}{dZ^2}+\left[\epsilon_0\frac{\omega^2}{c^2}-K_{||}^2\right]E_y(Z)+\frac{iB}{2q}\int_0^\infty dZ'\,E_y(Z')\exp(iq\mid Z-Z'\mid)=-iBD\exp(iqZ)-iBF\exp(-PZ) , \tag{36}$$

$$B=(\omega^2/c^2)4\pi\alpha_0M_\perp\omega_0/\hbar , \tag{37}$$

$$D=(q-iP)^{-1}\int_0^\infty dZ'[\tfrac{1}{2}+iP/2q)\exp(iqZ')-\exp(-PZ')]E_y(Z') , \tag{38}$$

$$F=(q-iP)^{-1}\int_0^\infty dZ'[\exp(-PZ')-\exp(iqZ')]E_y(Z') . \tag{39}$$

Equation (36) is very similar to Eq. (3.13a) of Ref. 3, apart from the terms with known spatial dependence in the right-hand side. We solve it by using the same method of Ref. 3. We apply the differential operator d^2/dZ^2+q^2 to both sides of Eq. (36) and obtain a differential equation:

$$\frac{d^4E_y(Z)}{dZ^4}+\left[q^2+\epsilon_0\frac{\omega^2}{c^2}-K_{||}^2\right]\frac{d^2E_y(Z)}{dZ^2}+\left[q^2\left[\frac{\epsilon_0\omega^2}{c^2}-K_{||}^2\right]-B\right]E_y(Z)=-iBF(q^2+P^2)\exp(-PZ) . \tag{40}$$

The general solution of this equation that is bounded as $Z\to\infty$ is

$$E_y(Z)=\mathscr{E}_1\exp(iq_1Z)+\mathscr{E}_2\exp(iq_2Z)-iBF(q^2+P^2)(q_1^2+P^2)^{-1}(q_2^2+P^2)^{-1}\exp(-PZ) , \tag{41}$$

where $\mathscr{E}_1$ and $\mathscr{E}_2$ are two constants to be determined, and q_1 and q_2 are the solutions of the equation

$$(q^2-q_i^2)\left[\frac{\epsilon_0\omega^2}{c^2}-K_{||}^2-q_i^2\right]=B \tag{42}$$

with $\mathrm{Im}q_i>0$, namely bulk-polariton wave vectors. The last term in (41) is a particular solution of the nonhomogeneous differential equation (40).

If we insert (41) into the original integro-differential equation (36), we find that the latter is satisfied only if $\mathscr{E}_1$ and $\mathscr{E}_2$ satisfy the condition

$$\frac{\mathscr{E}_1}{q_1-q}+\frac{\mathscr{E}_2}{q_2-q}=i[2qD-iBF(P-iq)(q_1^2+P^2)^{-1}(q_2^2+P^2)^{-1}] , \tag{43}$$

that plays the role of ABC. The unknowns quantities D and F can be computed by inserting Eq. (41) into their definitions (38) and (39). An inhomogeneous 2×2 linear system is obtained whose solution yields D and F. Then the electric field (41) and the ABC (43) take, respectively, the form:

$$E_y(z)=\sum_{i=1}^{2}\mathscr{E}_i[\exp(iq_iZ)+2P(P^2+q^2)(q_i^2-q^2)^{-1}(P-iq_i)^{-1}\exp(-PZ)] , \tag{41'}$$

$$\sum_{i=1}^{2}[q_i-i(\delta+P)](q_i^2-q^2)^{-1}(P-iq_i)^{-1}\mathscr{E}_i=0 , \tag{43'}$$

where

$$\delta=Pc^2\hbar(2\pi\alpha_0M_\perp\omega_0^3)^{-1}[(q_1^2+P^2)(q_2^2+P^2)+B] . \tag{44}$$

The electric field is a linear combination of two waves that, while reducing to bulk polaritons as Z increases, are modified in a depth of the order of $1/P$ below the surface. The ABC Eq. (43'), which depends on exciton parameters through P and δ, states that the resonant part of polarization vanishes at the surface.

The reflectivity is easily computed, matching the electric field inside the crystal given by Eqs. (41') and (35) to the external electric field

$$\mathscr{E}_y(Z)=\exp(-iK_{||}X)[\exp(iK_zZ)+r\exp(-iK_zZ)] , \tag{45}$$

where $K_z=\omega(\cos\theta)/c$, through Maxwell's boundary conditions, namely, for the s wave the continuity of $\mathscr{E}_y$ and $d\mathscr{E}_y/dZ$ for the surface. r, the complex reflectivity amplitude, is calculated after long but simple algebra:

$$r=[-(P+iK_z)+\mathscr{E}_1(P+iq_1)+\mathscr{E}_2(P+iq_2)](P-iK_z)^{-1} , \tag{46}$$

$$\mathscr{E}_1=2iK_z(q_1^2-q^2)(P-iq_1)(q_2-q-\gamma)D^{-1} . \tag{47}$$

$$\mathscr{E}_2=-2iK_z(q_2^2-q^2)(P-iq_2)(q_1-q-\gamma)D^{-1} , \tag{48}$$

$$\begin{aligned}D=&(q_2-q-\gamma)[-2P(P^2+q^2)(P-iK_z)+i(K_z+q_1)(q_1^2-q^2)(P-iq_1)]\\&+(q_1-q-\gamma)[2P(P^2+q^2)(P-iK_z)-i(K_z+q_2)(q_2^2-q^2)(P-iq_2)] ,\end{aligned} \tag{49}$$

$$\gamma=(q+iP)[2P(P+iq)\left[\frac{\epsilon_0\omega^2}{c^2}+P^2-K_{||}^2\right]/B-1] . \tag{50}$$

V. NORMAL-INCIDENCE REFLECTIVITY

A. Results

We calculate normal-incidence reflectivity from Eq. (46) for a broad range of physical situations. The difficulty is to handle the quite large number of parameters, namely ω_0, P, $4\pi\alpha_0$, ϵ_0, $M_\perp$, and Γ. Most of these parameters are not independent, for instance, ϵ_0 and $\hbar\omega_0$. We proceed as follows: First, we choose a very small value of Γ, but not zero, in order to avoid vanishing of the imaginary

parts of q_1 and q_2, since the computer must choose solutions of Eq. (42) with $\mathrm{Im}q_i > 0$. We use $\Gamma = 10^{-3}R^*$, that is smaller than 0.03 meV in all cases considered. Then we identify the main parameter of our approach, that is the ratio of dead layer depth $1/P$ to the inverse light wave vector in the medium. This parameter $\delta = (\omega/c)\sqrt{\epsilon_0}/P$, which describes the strength of the dead layer perturbation on light propagation, increases with decreasing exciton binding energy, that is with increasing dead layer depth. In Table I we report the relevant parameters for a number of semiconductors. We calculate the reflectivity for the extreme cases, $\delta = 0.046$ in CdS and $\delta = 1.25$ in InAs, and also for GaAs ($\delta = 0.17$), InP ($\delta = 0.13$), and ZnSe ($\delta = 0.083$). The values of ϵ_0, $M_\perp$, and $\hbar\omega_0$ are taken from Table I, while we consider in each case three values of $4\pi\alpha_0$, namely 10^{-3}, 3×10^{-3}, and 10^{-2}, to encompass the range of values quoted in the literature. Table I shows that spatial dispersion (M^{-1}) and dead layer effect (δ), though not strictly related, increase together. This occurs because quite flat bands (little dispersion) are often associated with large gaps and large exciton binding energy (small δ).

The reflectivity $R = |r|^2$ is shown in Figs. 3–5 as a function of $\hbar(\omega-\omega_0)$, respectively, for CdS, GaAs, and InAs. The results computed in the case of InP are qualitatively similar to those of GaAs, while those of ZnSe are similar to those of CdS. The curves of Figs. 3–5 encompass a broad range of physical situations and give quite a complete insight on exciton reflectivity in semiconductors. First we observe that the spike, frequently observed in reflectivity[16,19] at the longitudinal exciton frequency, never appears. This means that the intrinsic dead layer we consider is too small to generate it. We believe that the spike must be explained by extrinsic dead layers, rather than by some inadequacy of the approximations involved in this calculation.

Let us consider Fig. 3, where dead layer effects are the smallest. The effect of increasing oscillator strength, in addition to an obvious increase of reflectivity-structure amplitude, is a large shift of the dip to high energies, because of increasing longitudinal-transverse exciton separation, and a smaller high-energy shift of the maximum. Figures 4 and 5 show that the combined effects of spatial dispersion and dead layer drastically affect line shapes, especially those corresponding to large oscillator strength. Careful comparative examination of Figs. 3–5 shows that such effects are similar to those of decreasing oscillator strength, namely a shift of the structure to lower energies, and a reduction of the positive-negative peak ratio. Finally, it is worthwhile noticing that quantitative line shapes are sensitive even to small δ values. In fact, the ZnSe reflectivity, not shown in the figures, is appreciably different from CdS reflectivity,

TABLE I. Electron effective mass (m_e), hole effective mass (m_h), reduced mass (μ_0), exciton total mass (M), effective Rydberg (R^*), $n=1$ exciton resonance energy $E_0 = E_g - R^*$, and parameter $\delta = (\omega/c)\sqrt{\epsilon_0}/P$ describing the importance of dead layer effects, for a number of semiconductors. In the case of degenerate valence bands, m_h is the hole "spherical mass," defined in Ref. 47, and $M = m_e + m_h$ is an estimate of the exciton total mass. Data are from Ref. 47.

Material	m_e	m_h	μ_0	ϵ_0	R (meV)	M	E_g (eV)	δ
CdS	0.16	0.74	0.13	8.1	28	0.90	2.524	0.045
ZnS	0.39	0.42	0.20	8.1	42	0.81	3.758	0.059
CdTe	0.096	0.34	0.075	9.7	11	0.44	1.599	0.071
ZnSe	0.17	0.43	0.13	8.7	17	0.60	2.783	0.084
ZnTe	0.09	0.45	0.075	10.1	10	0.54	2.380	0.10
InP	0.077	0.16	0.052	12.1	4.9	0.24	1.305	0.13
GaAs	0.066	0.16	0.047	12.5	4.1	0.23	1.516	0.18
GaSb	0.047	0.11	0.033	15.2	2	0.16	0.808	0.18
InSb	0.015	0.041	0.011	16.8	0.5	0.056	0.240	0.18
GaP	0.013	0.195	0.078	11.1	8.6	0.21	2.731	0.22
Ge	0.038	0.082	0.026	15.4	1.5	0.12	0.889	0.26
AlSb	0.011	0.11	0.01	9.9	1.4	0.12	2.219	0.50
InAs	0.024	0.058	0.017	11.8	1.7	0.089	0.408	1.25

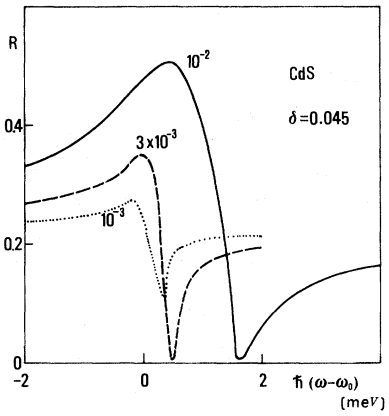

FIG. 3. Theoretical reflectivity computed for CdS as described in the text for $4\pi\alpha_0=10^{-2}$, 3×10^{-3}, 10^{-3}.

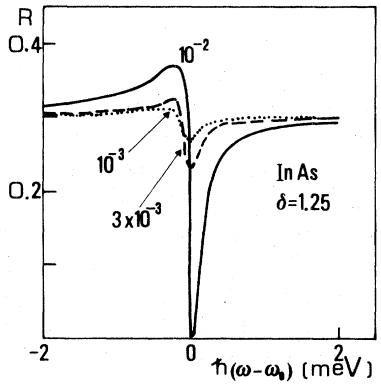

FIG. 5. Theoretical reflectivity computed for InAs as described in the text for $4\pi\alpha_0=10^{-2}$, 3×10^{-3}, 10^{-3}.

even though both involve very small δ values and very similar $M_\perp$ and ϵ_0 values.

B. Comparison with experiments

1. CdS

We compare our results with the experimental data of Evangelisti *et al.*[16], namely with the spectrum shown in the second curve (from the top) in Fig. 3 of Ref. 16. This spectrum is expected to be very close to the flat band condition (namely, no surface electric field), since it has the maximum amplitude of the $n=2$ exciton structure.[16] This choice should avoid surface electric fields, not considered in the theory, which may ionize excitons and give rise to extrinsic dead layers. Furthermore, an inhomogeneous electric field would attract excitons toward the surface (where the field is stronger), and the competition between both effects may affect reflectivity line shapes in an unpredictable way. We fit the experimental data varying only ω_0, $4\pi\alpha_0$, and Γ. We use the value $M_\perp=0.94$ (effective masses are measured in free-electron mass units) from Brillouin scattering experiments,[36] $\epsilon_0=8.0$ and $R^*=25$ meV from Ref. 16. Figure 6 shows the good agreement we find with experiments. The fit parameters $\hbar\omega_0=2.552$ eV, $4\pi\alpha_0=0.85\times10^{-2}$, $\Gamma=0.34$ meV are in reasonable agreement with values quoted in the literature,[16,22–24] although the first and second one are somewhat smaller. We believe our parameters to be more reliable than others that are determined in the homogeneous dead layer approximation.

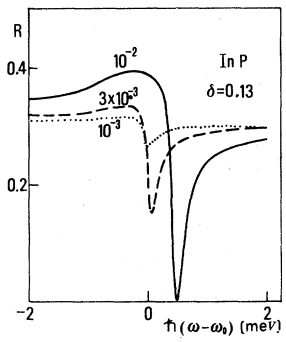

FIG. 4. Theoretical reflectivity computed for InP as described in the text for $4\pi\alpha_0=10^{-2}$, 3×10^{-3}, 10^{-3}.

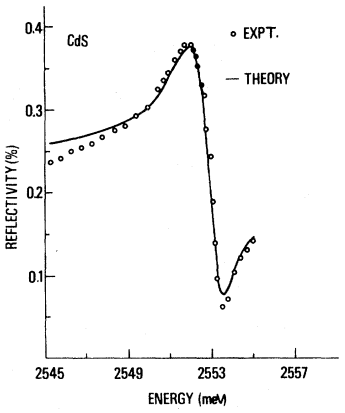

FIG. 6. CdS exciton reflectivity. Experimental data from Ref. 16. The solid curve is the fit computed according to the present theory with $\epsilon_0=8.1$, $M_\perp=0.94$, $R^*=29$ meV, $\hbar\omega_0=2.55$ eV, $4\pi\alpha_0=0.85\times10^{-2}$, $\Gamma=0.34$ meV.

2. GaAs

We apply this theory also to GaAs, InP, and ZnSe which have degenerate valence bands, even though it has been carried out just for single bands. In this case, two exciton branches appear[37] with the same binding energy, but different total mass, namely heavy (M_h) and light (M_l) excitons. However, Sell *et al.*[19] computed exciton reflectivity in GaAs in the homogeneous dead layer approximation and showed that it is quite well reproduced by a single exciton branch with $M=M^*$, where

$$M^{*-1}=(M_h^{-1}+M_l^{-1})/2\ . \tag{51}$$

On this ground and in order to avoid complications introduced in our theory by two exciton branches, we fit reflectance spectra of these materials using a single exciton branch with total mass M^*, in the spirit of ascribing otherwise unexplicable discrepancies to band degeneracy.

We consider GaAs exciton reflectivity measured by Sell *et al.*[19] and choose the spectrum of sample 40 in Fig. 4 of Ref. 19. We have already shown that the spike at the longitudinal-exciton frequency should be a consequence of extrinsic dead layers (or surface roughness[38]), and therefore choose this spectrum, since it shows the smallest spike. We fix the values $R^*=4.1$ meV, $\epsilon_0=12.6$, and $M^*=0.298$,[19,39] and find the best fit (Fig. 7, broken line) for $\hbar\omega_0=1.5150$ eV, $4\pi\alpha_0=0.22\times10^{-2}$, and $\Gamma=0.035$ meV. ω_0 agrees perfectly with the values quoted in the literature,[19,40,41] Γ is in reasonable agreement with them, and $4\pi\alpha_0$ is somewhat larger than the values obtained from absorption data (0.16×10^{-2}).[19,42]

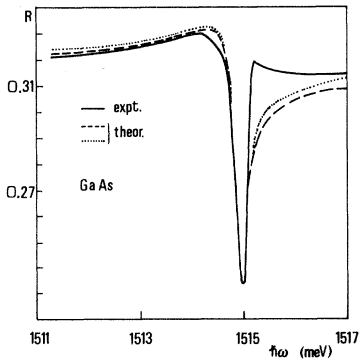

FIG. 7. GaAs exciton reflectivity. Experimental data from Ref. 19. Computed curves: dotted line, $\epsilon_0=12.8$, $M^*=0.23$, $R^*=4.2$ meV, $\hbar\omega_0=1514.8$ meV, $4\pi\alpha_0=0.21\times10^{-2}$, $\Gamma=0.01$ meV. Broken line, $\epsilon_0=12.6$, $M^*=0.298$, $R^*=4.2$ meV, $\hbar\omega_0=1515$ meV, $4\pi\alpha_0=0.22\times10^{-2}$, $\Gamma=0.035$ meV.

Apart from the spike, which cannot be reproduced by this theory, the fit is not satisfactory on the high-energy side, where the computed reflectivity is systematically lower than the experimental reflectivity. We believe that this is caused (at least partially) by neglecting the ω dependence of the background dielectric function $\epsilon_0(\omega)$, which includes the contribution of higher exciton states. We estimate the order of magnitude of their ω-dependent contribution, representing higher exciton states as a single oscillator resonant at $\omega_g=\omega_0+R^*/\hbar$, with the same oscillator strength as the exciton ground state. In this way we find that $\epsilon_0(\omega)$ and the computed reflectivity increase on the high-energy side by the exact amount needed to reproduce the experimental reflectivity at $\hbar\omega=1517$ meV.

The agreement between theory and experiment is better if ϵ_0 and M^* are changed slightly. Choosing $\epsilon_0=12.8$ and $M^*=0.23$, we find $\Gamma=0.01$ meV, $4\pi\alpha_0=0.21\times10^{-2}$, and unchanged ω_0, and the fit is improved on the high-energy side (dotted curve in Fig. 7). However, we do not trust this improvement, since the energy dispersion of the polarizability of higher exciton states should be revealed in some way. It must be remarked that this theory reproduced reflectivity line shapes in two very different cases as CdS (small dead layer) and GaAs (large dead layer) without taking the dead layer depth as an adjustable parameter.

3. InP

We fit experimental data of Evangelisti *et al.*[18] taken at 2 K, using $R^*=4.9$ meV, $\epsilon_0=12.1$,[18] and $M^*=0.3$.[39] The best fit was obtained (Fig. 8) with the parameters $\hbar\omega_0=1.4183$ eV, $4\pi\alpha_0=0.3\times10^{-2}$, and $\Gamma=0.01$ meV. The experimental data are reproduced better than in the case of GaAs, because of the absence of the spike. The low- and high-energy nearly-constant discrepancies can be at least partially ascribed to having neglected energy dispersion of the polarizability of higher exciton states. A slightly better fit, not shown in Fig. 8 but already reported in Ref. 26, is obtained if small adjustments of R^* (5.6 meV) and M^* (0.25) are allowed, leading to $\hbar\omega_0=1.4184$, $4\pi\alpha_0=0.29\times10^{-2}$, $\Gamma=0.004$ meV. As a trend, the fit improves as M^* decreases. In fact, we tried to use the value $M^*=0.53$, computed according to Eq. (51), from recent magnetoreflectance data,[39] but we were not

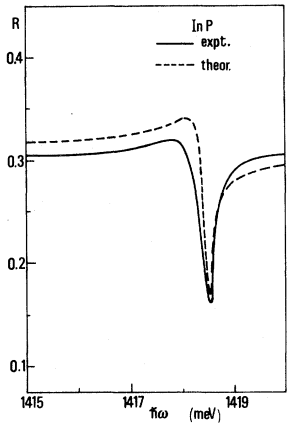

FIG. 8. InP exciton reflectivity. Experimental data from Ref. 18. Theoretical curve: $\epsilon_0=12.1$, $M^*=0.3$, $R^*=4.9$ meV, $\hbar\omega_0=1418.3$ meV, $4\pi\alpha_0=0.31\times10^{-2}$, $\Gamma=0.015$ meV.

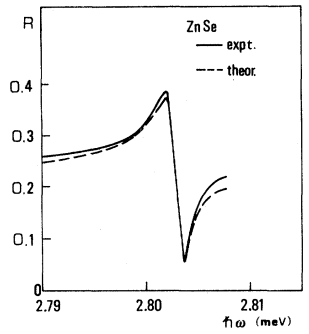

FIG. 9. ZnSe exciton reflectivity. Experimental data from Ref. 21. Theoretical curve: $\epsilon_0=8.1$, $M^*=0.6$, $R^*=21.2$ meV, $\hbar\omega_0=2802$ meV, $4\pi\alpha_0=0.88\times10^{-2}$, $\Gamma=0.2$ meV.

able to reproduce the experimental line shape. The low-energy positive peak becomes higher, narrower, and slightly shifted to higher energies with respect to the experimental data. This failure could be ascribed to the inadequacy of the single exciton-branch approach, but could bring some doubt on the reliability of valence-band parameters determined in Ref. 39.

4. *ZnSe*

We fit exciton reflectivity data of Feierabend and Weber[21] using $\epsilon_0=8.1$,[43] $M^*=0.57$, computed from Brillouin scattering experiments[44] according to Eq. (51), and $R^*=21.2$ meV, computed from $\epsilon_s=8.66$ (static screening)[45] and $\mu=0.12$.[45] We do not use the measured value $R^*=17$ meV,[45] since it is probably affected by polaron shift, as Venghaus[45] suggests in order to explain discrepancy with the computed value. The best fit (Fig. 9) is achieved for $\hbar\omega_0=2.8020$ eV, $4\pi\alpha_0=0.39\times10^{-2}$, and $\Gamma=0.2$ meV and is fairly satisfactory, not showing the discrepancies present in the case of GaAs and InP. The longitudinal-transverse splitting, determined from the above values of ϵ_0 and $4\pi\alpha_0$, is 0.7 meV, in good agreement with the experimental value 0.9 ± 0.2 meV.[44] Such agreement seems to confirm that the GaAs and InP discrepancies result from the neglect of the energy dependence of the polarizability of higher exciton states (in addition to extrinsic dead layers), rather than to valence-band degeneracy. In fact, the former effect should be negligible in ZnSe and CdS, where $n=2$ excitons are, respectively, 13 (Ref. 45) and 21 meV above the $n=1$ level, but not in GaAs and InP, where the separation of the first two exciton states is of the order of 3 meV, comparable with the amplitude of the energy range of Figs. 7 and 8.

VI. DISCUSSION

We have calculated Wannier-exciton wave functions in semi-infinite crystals and optical reflectivity from them. Of course, several assumptions are involved in this calculation. First, we use the boundary condition (3), leading to the "dead layer," that has been derived schematizing the vacuum crystal interface as an infinite energy barrier at the surface, with the perfect crystal potential just inside. Recent calculations[32] which neglect the image potential showed that the microscopic structure of the surface can alter this picture, leading to an accumulation layer of excitons, if surface states are present inside the gap. However, we believe that the effect of surface states on *bulk* excitons should be smaller, because of the long-range image potential, that repels electrons and holes from the surface, and should prevent them from feeling the short-range surface-state attractive potential. We also neglected the effect of built-in electric fields that could affect exciton motion both by ionizing them near the surface, e.g., introducing an extrinsic dead layer and attracting excitons toward the surface where the field is larger. Though difficult, it should be interesting to study this situation, because the interplay of attractive (short-range surface potential, field inhomogeneity) and repulsive

(image potential) surface forces could strongly affect exciton reflectivity.[46] In this study, we assume flat bands up to the surface, an experimental condition that could be controlled in principle. Even if this condition has never been rigorously tested for all experiments we consider, in the case of CdS we tried to reproduce the experimental spectrum[16] expected to approach it closely, as explained in Sec. V B. In the spirit of neglecting the microscopic structure of the surface, we also neglect surface roughness.[38]

The other assumptions, namely to neglect the image potential and the use of the analytical approximation for exciton wave functions, have been found to be justfied in the paper and should not affect our calculations in a qualitative way. One may expect our dead layer to be slightly underestimated because of neglecting the image potential, as shown in Ref. 14. Minor assumptions, performed for the sake of simplicity, have been to neglect the frequency dependence of the nonresonant polarizability and the band degeneracy. The former has been shown to affect agreement with experiments in quite a recognizable way.

Though involving these more or less justified assumptions, our theory is able to reproduce experimental reflectivity line shapes in a broad range of physical situations from relatively strong exciton binding (CdS) with a small dead layer to that of poorly bounded excitons (GaAs and InP) with large dead layers by varying only a few parameters, namely the exciton resonance frequency ω_0, oscillator strength $4\pi\alpha_0$, and lifetime broadening Γ. We never found normal-incidence reflectivity structures with the spike at the longitudinal exciton frequency and therefore ascribe it, when present in experiments, as in the case of GaAs, to extrinsic dead layers. This is substantiated by the fact the spike is not found in InP, whose intrinsic exciton parameters are very similar to those of GaAs.

The microscopic calculation shown in this paper confirms the existence of the dead layer or, more precisely, of a transition layer, of the order of $(\mu/M)^{1/2}a_B$, where exciton wave functions (and polarizability) are smaller than in the bulk. Since this is clearly an order-of-magnitude estimate, there is no discrepancy with previous estimates of about $2a_B$, based on the homogeneous dead layer approximation.[14,18] On the other hand, it should be emphasized that our dead layer is related to the exciton polarizability $\chi(Z,Z')$, while that of Refs. 14 and 18 are related to exciton polarization $P(Z)=\int_0^\infty dZ'\chi(Z,Z')E(Z')$, so that one must not expect them to be the same thing, in view of the strong nonlocal character of exciton polarizability.

ACKNOWLEDGMENTS

The authors thank Dr. G. B. Bachelet for help in drawing the curves of the image potential of Figs. 1 and 2. They are also indebted to Dr. F. Evangelisti for fruitful discussions. One of the authors (R.D.S.) thanks the Xerox Palo Alto Research Center for the use of its facilities in preparing the final version of the paper.

APPENDIX

In this appendix we show that the wave function (5) is correctly normalized. Since the $\vec{R}_{||}$-dependent part is already normalized to $\delta(\vec{K}_{||}-\vec{K}'_{||})$, it is sufficient to show that the $\psi(\vec{r},Z)$'s are normalized to $\delta(K_z-K'_z)$; that is

$$\int_0^\infty dZ\int_{-M_\perp Z/m_h}^{M_\perp Z/m_e} dz\int d^2r_{||}\psi'^*(\vec{r},Z)\psi(\vec{r},Z) =\delta(K'_z-K_z)\ ,$$

where Z is the exciton center-of-mass coordinate, and $\vec{r}=(\vec{r}_{||},z)$. ψ is a wave function of energy E, satisfying the equation

$$\left[-\frac{\hbar^2}{2\mu}\Delta_r-\frac{\hbar^2}{2M_\perp}\frac{\partial^2}{\partial Z^2}-\frac{e^2}{\epsilon r}\right]\psi=E\psi\ , \quad \text{(A1)}$$

and ψ' of energy E', satisfying a similar equation. If we multiply Eq. (A1) by ψ'^*, and the analogous equation for ψ'^* by ψ, and subtract, we get

$$(E'-E)\psi'^*\psi=-\frac{\hbar^2}{2\mu}(\psi\Delta_r\psi'^*-\psi'^*\Delta_r\psi) -\frac{\hbar^2}{2M_\perp}\left[\psi\frac{\partial^2}{\partial Z^2}\psi'^*-\psi'^*\frac{\partial^2}{\partial Z^2}\psi\right].$$

Now we integrate in the region $0\le Z\le L$, $r_{||}<\infty$, $-M_\perp Z/m_h\le z\le M_\perp Z/m_e$, and let L tend to infinity. The integral of the first term can be transformed at fixed Z, using Green's lemma, into an integral over the surface bounding the r-space volume. This integral vanishes because of boundary conditions (3) and the regularity of $\varphi_n(\vec{r})$ at infinity. The other integral can be performed first over Z, from the maximum between $m_e|z|/M_\perp$ and $m_h|z|/M_\perp$ to L, giving

$$(E'-E)\int_{\text{all space}} d^3r \int_0^\infty dZ\, \psi'^*\psi = -\hbar^2/2M_\perp \int_{\text{all space}} d^3r \left[\frac{\psi \partial \psi'^*}{\partial Z} - \psi'^* \frac{\partial \psi}{\partial Z} \right]_{Z=L} ,$$

so the only contribution to normalization is from the boundary $Z=L$. At $Z=L$, the evanescent waves do not contribute to the sum in (5), and ψ depends only on A. The integral on r is easily carried out, due to normalized property of φ_1. We get

$$\int_0^\infty dZ \int_{-M_\perp Z/m_h}^{M_\perp Z/m_e} dz \int d^2r_{||} \psi(\vec{r},Z)\psi'^*(\vec{r},Z) = -i[2\pi(1+|A|^2)(1+|A'|^2)]^{-1}$$
$$\times(\{\exp[i(K_z'-K_z)L]-A'^*A\exp[i(K_z-K_z')L]\}/(K_z'-K_z)$$
$$+\{A\exp[i(K_z+K_z')L]-A'^*\exp[-i(K_z+K_z']L)\}/(K_z'+K_z))$$
$$+a(L)\delta(K_z'-K_z) .$$

$a(L)$ must be zero, since the integral is a continuous function of K_z and K_z' at finite L.

When L tends to ∞, the integral is a rapidly oscillating function of K_z-K_z' and only the first term must be retained, since it is large at $K_z'=K_z$. In this case, A' can be replaced by A, and $A'^*A=|A|^2=1$ as is shown in parts C and D of Sec. II. The result is

$$\lim_{L\to\infty} \int_0^\infty dZ \int_{-M_\perp Z/m_h}^{M_\perp Z/m_e} \int d^2r_{||} \psi'^*(\vec{r},Z)\psi(\vec{r},Z) = \pi^{-1} \lim_{L\to\infty} (K_z'-K_z)^{-1}\sin[(K_z'-K_z)L]$$
$$=\delta(K_z'-K_z) ,$$

showing the correct normalization of (5).

[1]S. I. Pekar, Zh. Eksp. Teor. Fiz. 33, 1022 (1957) [Sov. Phys.—JETP 6, 785 (1958)]; Fiz. Tverd. Tela (Leningrad) 4, 1301 (1962) [Sov. Phys.—Solid State 4, 953 (1962)].

[2]J. J. Hopfield and D. G. Thomas, Phys. Rev. 132, 563 (1963).

[3]A. A. Maradudin and D. L. Mills, Phys. Rev. B 6, 2787 (1973).

[4]G. S. Agarwal, D. N. Pattanyak, and E. Wolf, Phys. Rev. Lett. 27, 1022 (1971); Opt. Commun. 4, 255 (1971); 4, 260 (1971).

[5]J. L. Birman and J. J. Sein, Phys. Rev. B 6, 2482 (1972).

[6]R. Zeyher, J. L. Birman, and W. Brenig, Phys. Rev. B 6, 4613 (1972).

[7]D. L. Johnson and P. R. Rimbey, Phys. Rev. B 14, 2398 (1976).

[8]M. R. Philpott, Phys. Rev. B 14, 3471 (1976).

[9]C. A. Mead, Phys. Rev. B 15, 519 (1977).

[10]C. A. Mead and M. R. Philpott, Phys. Rev. B 17, 914 (1978).

[11]C. A. Mead, Phys. Rev. B 17, 4644 (1978).

[12]C. S. Ting, M. J. Frankel, and J. L. Birman, Solid State Commun. 17, 1285 (1975).

[13]S. Sakoda, J. Phys. Soc. Jpn. 40, 152 (1976).

[14]I. Balslev, Phys. Status Solidi B 88, 155 (1978).

[15]D. C. Mattis and G. Beni, Phys. Rev. B 18, 3816 (1978).

[16]F. Evangelisti, A. Frova, and F. Patella, Phys. Rev. B 10, 4253 (1974).

[17]F. Patella, F. Evangelisti, and M. Capizzi, Solid State Commun. 20, 23 (1976).

[18]F. Evangelisti, J. U. Fischbach, and A. Frova, Phys. Rev. B 9, 1516 (1974).

[19]D. D. Sell, S. E. Stokowski, R. Dingle, and J. V. Di Lorenzo, Phys. Rev. B 7, 4568 (1973).

[20]K. Hümmer and P. Gebhardt, Phys. Status Solidi B 85, 271 (1978).

[21]S. Feierabend and H. G. Weber, Solid State Commun. 26, 191 (1978).

[22]W. Stössel and H. J. Wagner, Phys. Status Solidi B 89, 403 (1978).

[23]I. Broser, M. Rosenzweig, R. Broser, M. Richard, and E. Birkicht, Phys. Status Solidi B 90, 77 (1978).

[24]W. Stössel and H. J. Wagner, Phys. Status Solidi B 96, 369 (1979).

[25]W. Andreoni, M. De Crescenzi, and E. Tosatti, Solid State Commun. 26, 425 (1978).

[26]A. D'Andrea and R. Del Sole, Solid State Commun. 30, 145 (1979).

[27]C. B. Duke, Phys. Rev. 159, 632 (1967).

[28]R. Del Sole, J. Phys. C 8, 2971 (1975).

[29]R. Del Sole, Solid State Commun. 19, 207 (1976).
[30]R. Del Sole and D. E. Aspnes, Nuovo Cimento B 39, 791 (1977); Phys. Rev. B 17, 3310 (1978).
[31]M. F. Deigen and M. D. Glinchuk, Fiz. Tverd. Tela (Leningrad) 5, 3250 (1964) [Sov. Phys.—Solid State 5, 2377 (1964)].
[32]M. Altarelli, G. B. Bachelet, and R. Del Sole, J. Vac. Sci. Technol. 16, 1370 (1979); M. Altarelli, G. B. Bachelet, V. Bouché, and R. Del Sole (unpublished).
[33]R. J. Elliott, Phys. Rev. 108, 1384 (1957).
[34]F. Bassani and G. Pastori Parravicini, in *Electronic States and Optical Transitions in Solids,* edited by R. A. Ballinger (Pergamon, New York, 1975), p. 88.
[35]The latter limitation makes this approximation valid for not too large $M_\perp$ values, that is, complementary to the adiabatic approximation of Refs. 13 and 14, which is correct when $M_\perp$ tends to infinity.
[36]G. Winterling and E. Kotelès, Solid State Commun. 23, 95 (1977).
[37]E. O. Kane, Phys. Rev. B 11, 3850 (1975).
[38]R. Monreal, F. Garcia Molinear, and F. Flores, Solid State Commun. 32, 613 (1979).
[39]W. E. Ekardt, K. Lösch, and D. Bimberg, Phys. Rev. B 20, 3303 (1979).
[40]G. Fishman, Solid State Commun. 27, 1097 (1978).
[41]J. Lagois, E. Wagner, W. Bludau, and K. Lösch, Phys. Rev. B 18, 4325 (1978).
[42]M. D. Sturge, Phys. Rev. 127, 768 (1962).
[43]G. E. Hite, D. T. F. Marple, M. Aven, and B. Segal, Phys. Rev. 156, 850 (1967).
[44]B. Sermage and G. Fishman, Phys. Rev. Lett. 43, 1043 (1979).
[45]H. Venghaus, Solid State Commun. 26, 199, (1978).
[46]V. A. Kiselev, Fiz. Tverd. Tela (Leningrad) 20, 2173 (1978) [Sov. Phys.—Solid State 20, 1255 (1979)].
[47]A. Baldereschi and N. O. Lipari, Phys. Rev. B 3, 439 (1971).